International Conference on Fast Sea Transportation 2021
26-27 October 2021, Providence, RI

Computational Simulations of Wide-Beam Air-Cavity Hull in Waves

Konstantin. I. Matveev (V)
School of Mechanical and Materials Engineering, Washington State University, Pullman, WA, 99164, USA

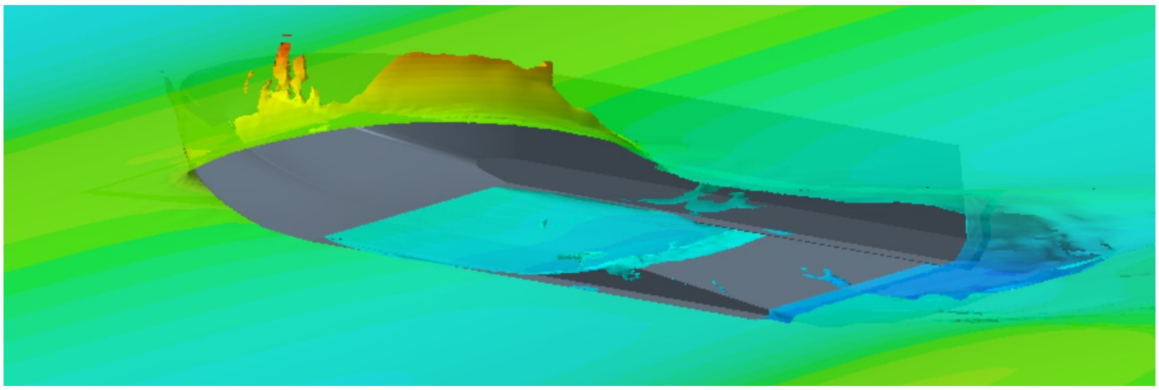

An effective method to reduce ship drag is to supply air under specially profiled bottom with the purpose to decrease wetted surface area of the hull and thus its water resistance. Although such systems have been installed on some vessels, the broad implementation of this technique has not yet occurred. A major problem is how to sustain air lubrication in rough water. Modeling of air-ventilated flows is challenging, but modern computational fluid dynamics tools can provide valuable insight. In this study, a wide-beam, shallow-draft hull with a bottom air cavity is considered. This hull imitates a semi-planing boat that can be used for fast transportation of cargo from large marine vessels to shallow shores. To simulate fluid flow around this hull in calm water and head waves, as well as heave and pitch motions of the boat, CFD software Star-CCM+ has been employed. It is found that the air cavity effectiveness decreases in waves; vertical accelerations exhibit high-frequency oscillations; and heave, pitch and vertical accelerations increase, while time-averaged heave, pitch and added drag show non-monotonic behavior with increasing wave amplitude. The air-cavity hull also demonstrates substantially lower vertical accelerations in waves in comparison with a similar solid hull without bottom recess. Time histories of kinematic parameters and distributions of flow field variables presented in this paper can be insightful for developers of air-cavity hulls.

KEY WORDS: Air-cavity ship; seakeeping; computational fluid dynamics.

INTRODUCTION

The development of systems that can lead to ship fuel savings, accompanied by decrease of pollutant emissions, is a part of global sustainability efforts in the maritime engineering industry. Reducing hydrodynamic drag of marine vessels can effectively address this goal. One of the methods that was proposed over a century ago but only recently started to appear on ships involves air injection under hull bottoms (Butuzov et al. 1981, Latorre 1997, Pavlov et al. 2020). Among several air-based methods, the formation of a continuous air cavity attracted significant attention in the past and is addressed in this paper. A concept of a hull with an air cavity formed inside a bottom recess is shown in Fig. 1.

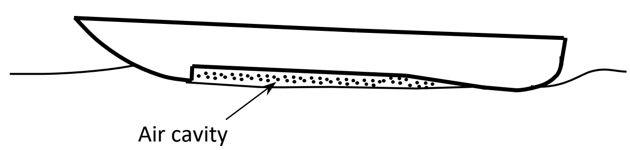

Fig. 1 Schematic of air-cavity boat.

The air lubrication of ship hulls primarily aims at reducing the frictional drag, as the wetted hull surface area decreases. Hence, it is especially attractive for slow displacement vessels and very fast planing boats, where frictional resistance is dominant. However, even for marine vehicles operating in semi-displacement and semi-planing modes, drag reduction (or speed increase) of even several percent is economically significant. Besides, air cavities can also lessen wave resistance, as the vessel draft will decrease with pressurized air cavities. This study focuses on a somewhat special wide-beam hull in a semi-planing regime, which applications can include high-speed transportation of volumetric cargo to or in shallow waters. However, such hulls may experience significant motions and hydrodynamic loads in the presence of waves in open water. The main goal of this work is to carry out exploratory numerical simulations of a basic wide-beam air-cavity hull in head waves to provide insight on the air-cavity boat dynamics and associated flow phenomena.

The hydrodynamic analysis of air-cavity ships in the past relied mainly on linearized potential-flow methods (Butuzov 1988, Matveev 2012). Although these models can be useful for predicting cavity shapes, the complexities of air-ventilated flows, including air leakage, non-linearities, turbulence and viscous effects, require more comprehensive computational fluid dynamics (CFD) tools for higher fidelity simulations. The CFD approach is much more numerically expensive, but the growth of computational resources made usage of these tools a common practice in the maritime industry. Several CFD simulations for air-cavity systems have been reported in recent years (e.g., Cucinotta et al. 2018, Hao et al. 2019). Although reasonable agreement with test data has been achieved in some situations, modeling issues still remain (e.g., Rotte et al. 2019, Mukha and Bensow 2020), such as the application of turbulence models for strongly disturbed surface flow in the cavity re-attachment zone.

Numerical modeling of air-cavity hulls in unsteady regimes is even more challenging. While the added-mass strip models commonly used for planing boats have been tried for air-cavity hulls as well (Matveev 1999), such methods can be treated as rather approximate. The present study attempts to apply high-fidelity CFD modeling for an air-cavity boat moving in waves. The present CFD approach has been validated for modeling of planing hull slamming (Matveev 2021).

It can be noted that the current topic has similarities with modeling of other air-assisted craft, such as air-cushion vehicles, surface-effect-ships and very fast multi-hulls (Faltinsen 2005, Yun and Bliault 2005, Matveev and Dubrovsky 2007), although air layers are much thicker in those situations. Moreover, traditional ships during slamming events can also undergo processes when an air layer, albeit much thinner in this case, is entrapped between flat bottoms and water (e.g., Lewison and Maclean 1968, Bertram 2000). The presence of air under hulls generally results in reduction of hydrodynamic loads on hulls during water entry. Drop experiments with prismatic air-cavity hull sections indicated almost twice lower peak accelerations in comparison with a solid body without bottom recess (Keehnel and Matveev 2014).

The next section of this paper outlines the utilized numerical method, boat hull geometry, computational setup, and mesh-verification study. It is followed by presentations of simulation results for an air-cavity hull in calm water and two head-wave conditions.

COMPUTATIONAL ASPECTS

Governing Equations and Turbulence Model

Numerical modeling of the flow around an air-cavity boat and two-degree-of-freedom (pitch and heave) motions of the hull was carried out in this project using the state-of-the-art CFD software Star-CCM+. A finite-volume segregated viscous solver with the 2nd-order discretization in space and the 1st-order implicit time stepping were employed. The water was treated as incompressible substance, whereas air was modeled as an ideal gas. The multiphase approach involving the volume-of-fluid (VOF) method was utilized (Hirt and Nichols 1981).

The governing Reynolds-averaged Navier-Stokes equations (RANSE) include the continuity and momentum equations,

$$\frac{\partial \rho}{\partial t}+\frac{\partial(\rho u_j)}{\partial x_j}=0\ , \tag{1}$$

$$\frac{\partial(\rho u_i)}{\partial t}+\frac{\partial(\rho u_i u_j)}{\partial x_j}=-\frac{\partial p}{\partial x_i}+\rho f_i+ \frac{\partial}{\partial x_j}\left[\mu\left(\frac{\partial u_i}{\partial x_j}+\frac{\partial u_j}{\partial x_i}-\frac{2}{3}\delta_{ij}\frac{\partial u_k}{\partial x_k}\right)-\rho\overline{u'_i u'_j}\right], \tag{2}$$

where u_i is the Reynolds-averaged velocity, ρ is the effective fluid density, p is the pressure, f is the body force, and $-\rho\overline{u'_i u'_j}$ is the Reynolds stress. The mixture density ρ and viscosity μ are calculated as $\rho=\rho_a\beta+\rho_w(1-\beta)$ and $\mu=\mu_a\beta+\mu_w(1-\beta)$, where β is the volume fraction of air, and indices a and w correspond to air and water, respectively.

To model effects of turbulence (i.e., the Reynolds stress), the all-Y+ realizable $k-\varepsilon$ model was employed (Rodi 1991), as it showed promising results in our previous simulations of air-cavity setups at high Reynolds numbers (Matveev and Collins 2021). This turbulence model is also one of most commonly used for CFD studies of ship hulls (De Luca et al. 2016). The time step in the present simulations was selected to keep the Courant number below one, which was also sufficient to resolve high-frequency oscillations during slamming events.

Hull Specifications and Numerical Domain

Although a number of publications on air-cavity hulls exist in the literature, exact geometric models of the tested hulls specific to this study are not publicly available. Thus, for the current exploratory simulation effort, a simple hull form was chosen based on a model-scale air-cavity hull that was built primarily for low-speed operations in the author's research group. The original displacement-type hull and its experimental realization are shown in Figs. 2a and 3. It has a barge-type geometry with somewhat refined bow.

The employed here CFD approach has been previously validated for this boat in the displacement and semi-displacement regimes (Collins et al. 2021). The experimental hull was instrumented with sensors measuring thrust, speed, trim and cavity pressure, as well as an onboard camera for video recording the air cavity shape through the transparent ceiling of the hull bottom recess.

The boat was tested in the length-based Froude number range between 0.17 and 0.5 under three loading conditions resulting in the zero, bow-up and bow-down static trim angles at rest. CFD simulations were conducted for the tested conditions using the same numerical approach as in the present study. All trends of measured variables were correctly predicted, and reasonable quantitative agreement was found (Collins et al. 2021). With increasing hull speed, drag and trim values increased while cavity length and pressure generally decreased.

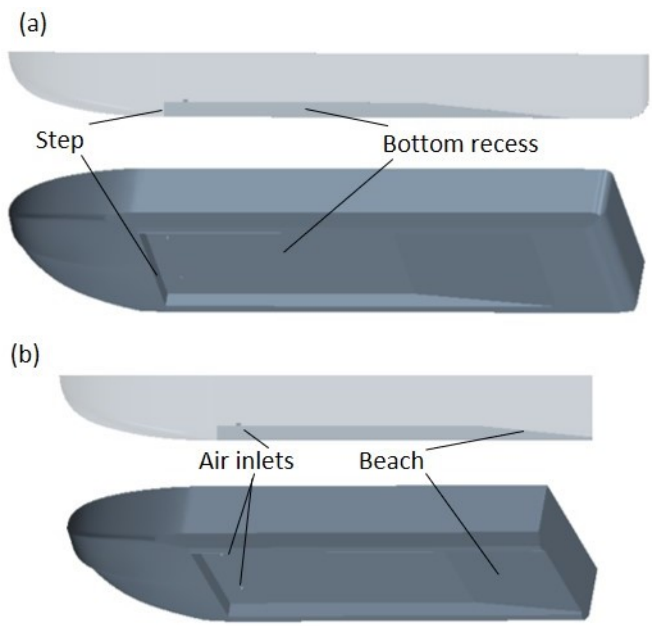

Fig. 2 (a) Original displacement hull used in lower-speed experiments and (b) semi-planing hull modification utilized in the present computational study.

Fig. 3 Instrumented displacement-type air-cavity boat on water.

To make the previously studied hull more suitable for higher-speed simulations of semi-planing regimes, a stern part of this hull was removed in the CAD software, and the remaining hull was adopted for the current numerical study. (Such a transformation has not been accomplished with the real experimental boat.) This "virtual" high-speed hull with transom stern is depicted in Fig. 2b. Its main specifications selected for CFD simulations are listed in Table 1. Two air inlets of diameter 0.01 m are located on the bottom recess ceiling at 0.05 m behind the step and 0.08 m away from the centerline. It should be noted that this hull is not hydrodynamically optimized, as the main purpose here is to obtain simulation data with a basic hull form rather than aim at developing a high-performance air-cavity boat with complex geometry.

Table 1. Main parameters of modified semi-planing hull.

Mass	16.8 kg
Length	1.23 m
Beam	0.4 m
LCG from transom	0.46 m
Inertia moment about transverse axis	1.6 kg·m^2
Bottom recess length (step position from transom)	0.87 m
Recess width	0.3 m
Step height	0.035 m

The numerical domain was built up around this hull, as shown in Fig. 4. The domain length, half-width and height are equal to 17.5, 3.75 and 6.7 of the hull beams, respectively. One of the vertical sides of the domain, passing through the hull centerplane, is treated as a symmetry plane, which allows us to simulate flow only in the half of the domain and thus reduce computational cost. The other boundary conditions included velocity inlets on the planes in front, behind, below and on top of the hull. The external flow conditions were assigned at these boundaries, corresponding to either uniform wind-current flow in the calm-water case or head waves plus steady wind-current in wave conditions. The other side boundary of the domain (parallel to the incident flow) was modeled as a slip wall, whereas the hull surface was considered as a no-slip wall, except for the air inlet that was treated as an inlet with prescribed velocity. In order to model pitch and heave motions of the hull, another boundary, the so-called overset surface, was assigned on the rectangle surrounding the hull, where solutions from the near-hull region and outside region were matched. This allows the overset region to move together with the hull inside the stationary background region.

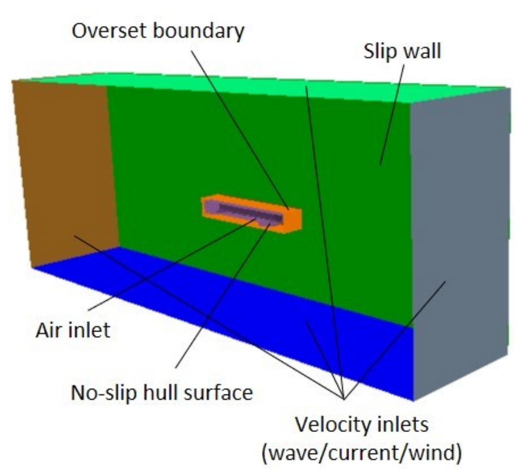

Fig. 4 Numerical domain with boundary conditions.

Meshing and Mesh-Verification Study

The numerical grids, consisting primarily of hexahedral cells, were built for both the background region, spanning the numerical domain, and the overset region, around the hull. Mesh refinements were implemented near the free surface, around the hull, and especially in the recess region, where the air cavity is present. In addition, prism layers were created on the hull surface with the near-wall numerical thickness mainly between 30-80 of Y+ values, thus relying on the wall function methodology. Illustrations of the fine numerical grid are shown in Fig. 5.

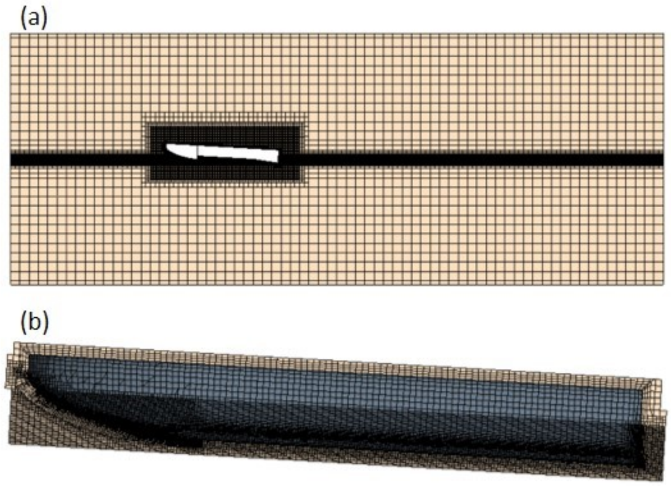

Fig. 5 (a) Mesh in the vertical plane of the entire numerical domain (excluding hull). (b) Mesh in the vertical plane and on the hull surface inside the overset region.

Table 2. Numerical results obtained on different grids and estimated numerical uncertainties. (Heave values are relative to the hull position at rest).

Mesh	Drag	Trim	Heave
Coarse	29.6 N	2.75°	3.79 cm
Medium	24.6 N	3.10°	4.13 cm
Fine	24.4 N	3.28°	3.95 cm
Numerical uncertainty (in % of fine-mesh solution)	1%	12%	11%

In general, using finer numerical grids can provide better resolution of the flow features, but this also increases computational cost. In order to achieve mesh-independent results for important hydrodynamic characteristics of the hull, a mesh-dependency study was conducted in the calm-water condition for the semi-planing hull at the volumetric Froude number of 2.21. The results obtained on three grids of different density are summarized in Table 2. The monotonic convergence is observed for drag and trim values, while oscillatory convergence is found for heave. Using these results, the standard procedure has been applied to assess numerical uncertainties (ITTC 2008). The resulting uncertainty values are listed in Table 2, and they are deemed acceptable for the present investigation.

RESULTS

Numerical simulations were conducted with the adapted hull geometry at speed of 3.5 m/s in calm water and in two regular head wave conditions: with wavelength close to the hull length, $\lambda = 1.09L$, and twice that number, $\lambda = 2.18L$. The corresponding hull length and displacement Froude numbers were 1.01 and 2.21, respectively, which indicate that the hull was moving in the semi-planing mode. The forward horizontal speed was kept constant, thus ignoring surge motions which could be significant in real conditions with large waves. The wave height was selected as 1/30 of the wave length, thus making the wave height twice bigger in longer waves.

The air supply rate Q was kept constant at 0.42 L/s, which corresponded to the non-dimensional flow rate $C_Q = Q/(U h_r B_r)$ of about 0.023, where U is the hull speed, and h_r and B_r are the step and width the bottom recess, respectively. This value is comparable with that used in large laboratory air-cavity systems of similar kind (Ceccio 2010). The nominal required power for air supply is evaluated to be below 1% of the propulsion power in the steady-state calm-water condition.

The results obtained for the time-averaged hydrodynamic characteristics in both calm water and waves are listed in Table 3, illustrations of flow field variables are presented in Figs. 6 and 9-12, and time histories of boat variables in nearly repeatable cycles in waves are shown in Figs. 7-8. The monitored characteristics included heave h and pitch τ of the hull, vertical accelerations a_z at the center of gravity, and the horizontal drag force D. The heave values in Table 3 are given in reference to the boat position at rest when no air is present underneath the hull. In Figs. 7-8, heave is normalized by the hull beam B, acceleration by the gravity constant g, and instantaneous drag is divided by the hull resistance D_0 in calm water (given in Table 3).

Table 3. Time-averaged characteristics in calm water and waves.

	Calm water	Head waves, $\lambda = 1.09L$	Head waves, $\lambda = 2.18L$
Heave	3.95 cm	3.67 cm	4.37 cm
Pitch	3.28°	2.71°	3.43°
Drag	24.4 N	30.2 N	29.3 N

In calm water, the boat trims at about 3° (Fig. 6a) with drag-to-weight ratio near 0.15 (Table 3). Most of the bottom recess is filled with air (Fig. 6b). Air is escaping from both the tail part of the cavity and under the side skegs, indicating that flow rate could be further reduced. However, since the power for pumping air is small, some air-supply margin is beneficial to compensate for larger air leak in case of disturbances. One can notice that the skin friction coefficient is close to zero in the zone covered by the air (Fig. 6d). The pressure reaches maximum in the water impingement region on the bow piece (Fig. 6c), while smaller zones with elevated pressure are present right behind the cavity reattachment, where the water flow also impinges on the hull. The pressure coefficient in the air cavity is greater than zero (in contrast to natural ventilation), which indicates that the cavity contributes to the lift force supporting a part of the boat weight.

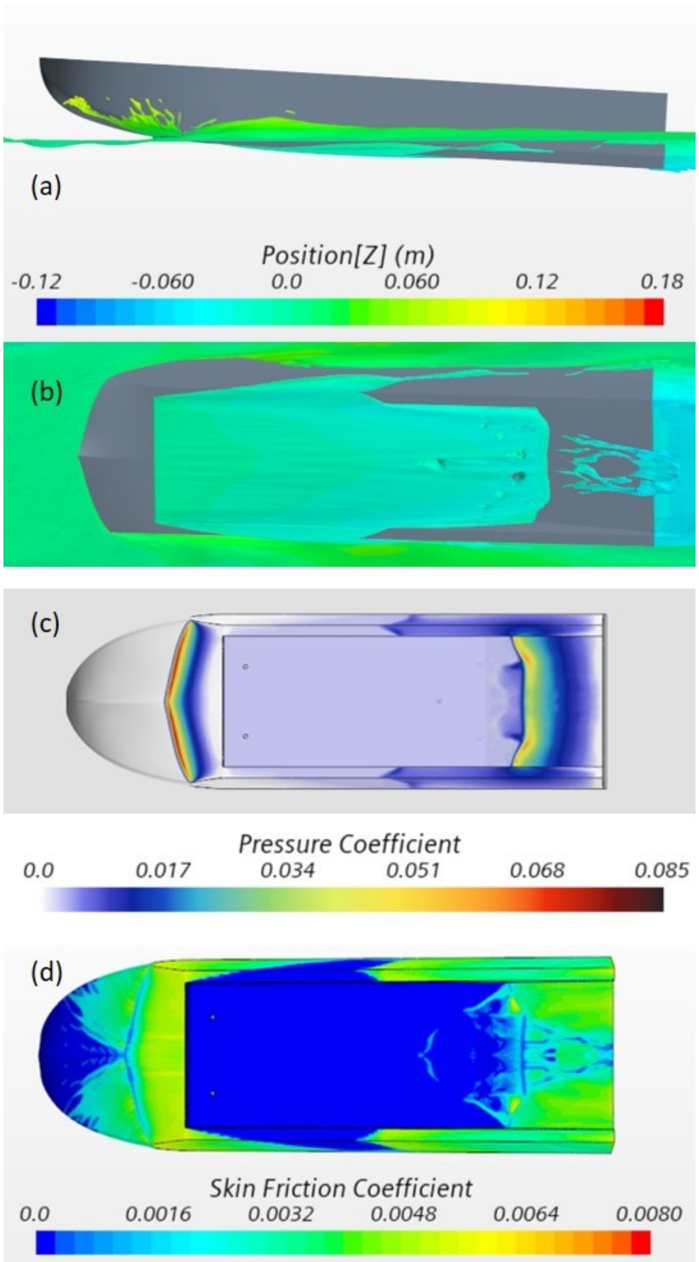

Fig. 6 (a,b) Steady-state hull positions and water surface elevations in calm water: (a) side view and (b) underwater view. (c,d) Distributions of (c) pressure coefficient and (d) skin friction coefficient on the hull surface.

Numerical results for the case with moderate waves ($\lambda = 1.09L$) are given in Figs. 7 and 9-10. The heave and pitch of the hull show regular oscillations with modest nonlinearity (Fig. 7a,b). The acceleration signal manifests noisier behavior with noticeable oscillations in the acceleration-receding part of the cycle (Fig. 7c). These oscillations occur at a frequency of about 35 Hz, which is comparable with an estimate for the lowest natural frequency of an air cavity (Keehnel and Matveev 2014). Thus, it can be hypothesized that hull motions lead to excitations of the air cavity oscillations. Anyway, at this speed and wave, these oscillations are not always pronounced as can be seen in the second cycle showing much smaller oscillations (Fig. 7d). The drag force shows drastic increase well correlated with the acceleration growth (Fig. 7d,e). The force recedes faster after reaching the peak; and in some parts of the cycle, resistance drops below the calm-water drag.

Illustrations of the field variables at three instances in the motion cycle (indicated by vertical dashed lines in Fig. 7) are presented in Figs. 9-10. The first time moment corresponds to the lowest (negative) vertical acceleration, when the bow exits the wave crest (Fig. 9a). The second instance is at the highest (positive) acceleration, when the bow enters the water. The third point is for the hull climbing up through the next wave.

The underwater views show only a small wetted area of the hull in front of the air cavity at time 10 s, while the cavity becomes shorter at the relatively large pitch, and noticeable amount of air is shed downstream (Fig. 9b). At about 10.1 s, larger bow area appears in the water, entraining some air, while the cavity is longer due to lower pitch. Close to 10.2 s, the cavity shortens, whereas some air just has moved behind the cavity tail.

The pressure maps (Fig. 10a) indicate decreased pressure coefficient at the bow when it passes a wave crest, followed by a drastic pressure rise in a localized impingement zone on the bow, when the bow re-enters water. As the hull goes through the next wave, the highest-pressure areas form behind the cavity. One can note that pressure coefficient inside the air cavity is close to zero in all instances, which suggests that the cavity loses its lifting capability in this wave condition. This is in agreement with lower vertical position of the hull relative to the calm-water value (Table 3). The local friction coefficient patterns (Fig. 10b) are consistent with the water interfaces (Fig. 10b), so near-zero friction appears on dry hull surfaces, and the largest friction coefficient values are present in the third phase when the boat climbs upon the wave.

Simulations carried out in larger waves show bigger nonlinearities in hull motions and flow. With doubling the wavelength and height, heave and pitch oscillation amplitudes increase about 10 and 5 times, respectively (Fig. 8a,b). The peak accelerations also increase about an order of magnitude in comparison with smaller waves (Fig. 8c). High-frequency oscillatory behavior now appears immediately after the peak acceleration, while their frequency remains about the same. This again points to excitation of the air cavity oscillations. The dynamic behavior of the hull resistance can also be correlated with acceleration dynamics, including highly oscillatory region (Fig. 8d). However, one can also notice the pronounced negative drag peak preceding the sharp rise, and more gradual decrease of the resistance following the oscillatory interval.

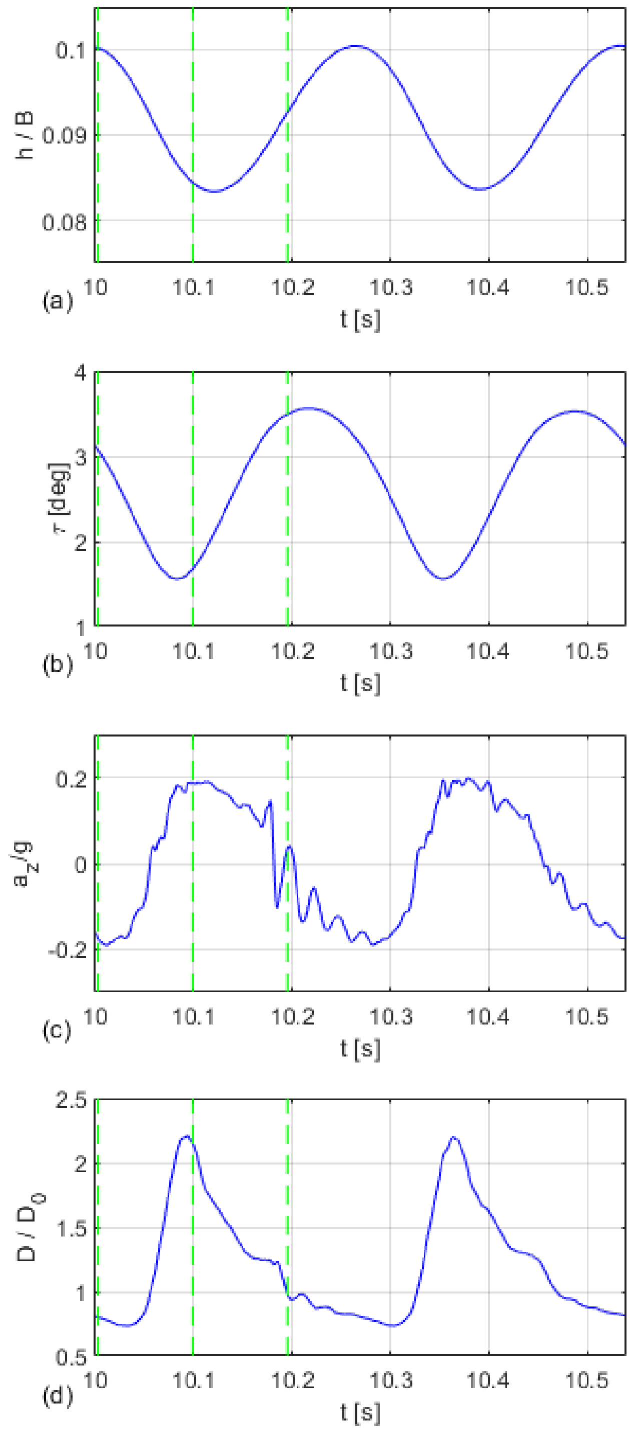

Fig. 7 Time-dependent results for (a) heave, (b) pitch, (c) vertical acceleration and (d) drag in head waves with $\lambda = 1.09L$. Vertical dashed lines indicate time moments for which flow field variables are presented in Figs. 9-10.

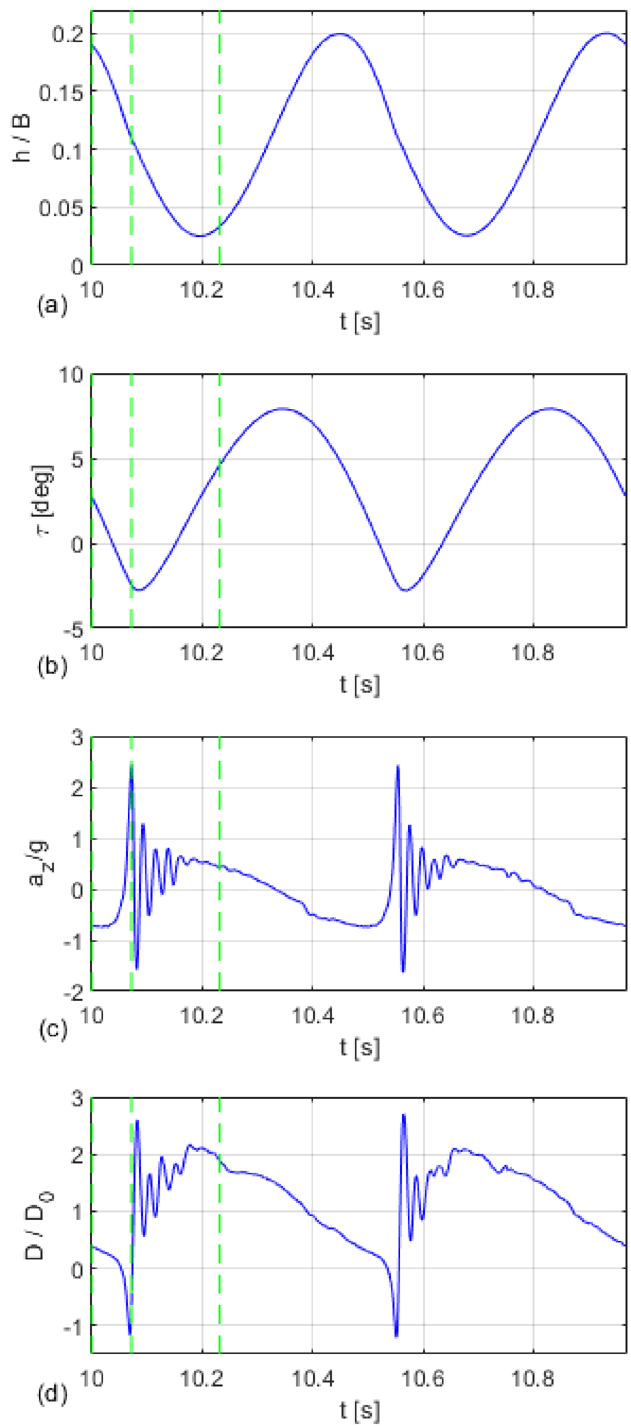

Fig. 8 Time-dependent results for (a) heave, (b) pitch, (c) vertical acceleration and (d) drag in head waves with $\lambda = 2.18L$. Vertical dashed lines indicate time moments for which flow field variables are presented in Figs. 11-12.

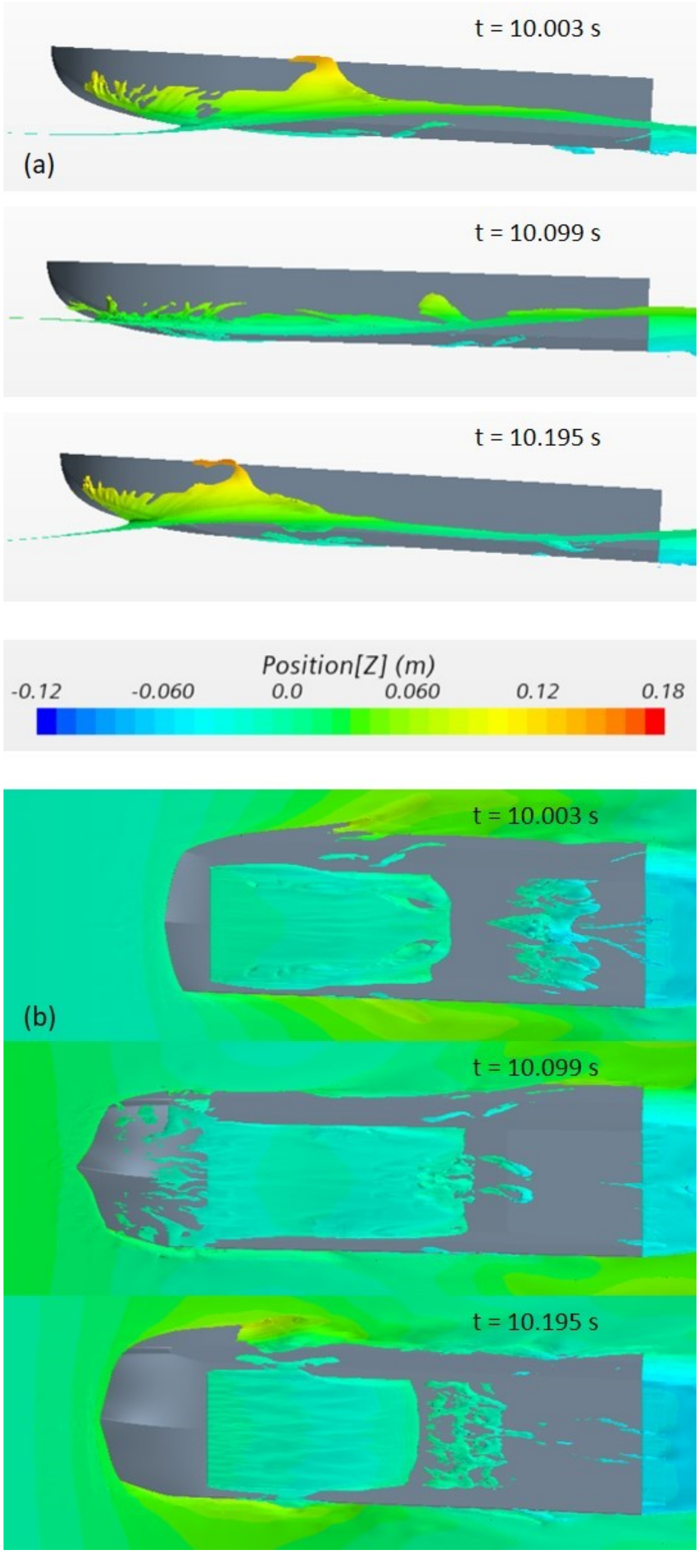

Fig. 9 Hull positions and wave surface elevations at three time instances in head waves with $\lambda = 1.09L$: (a) side view and (b) underwater view.

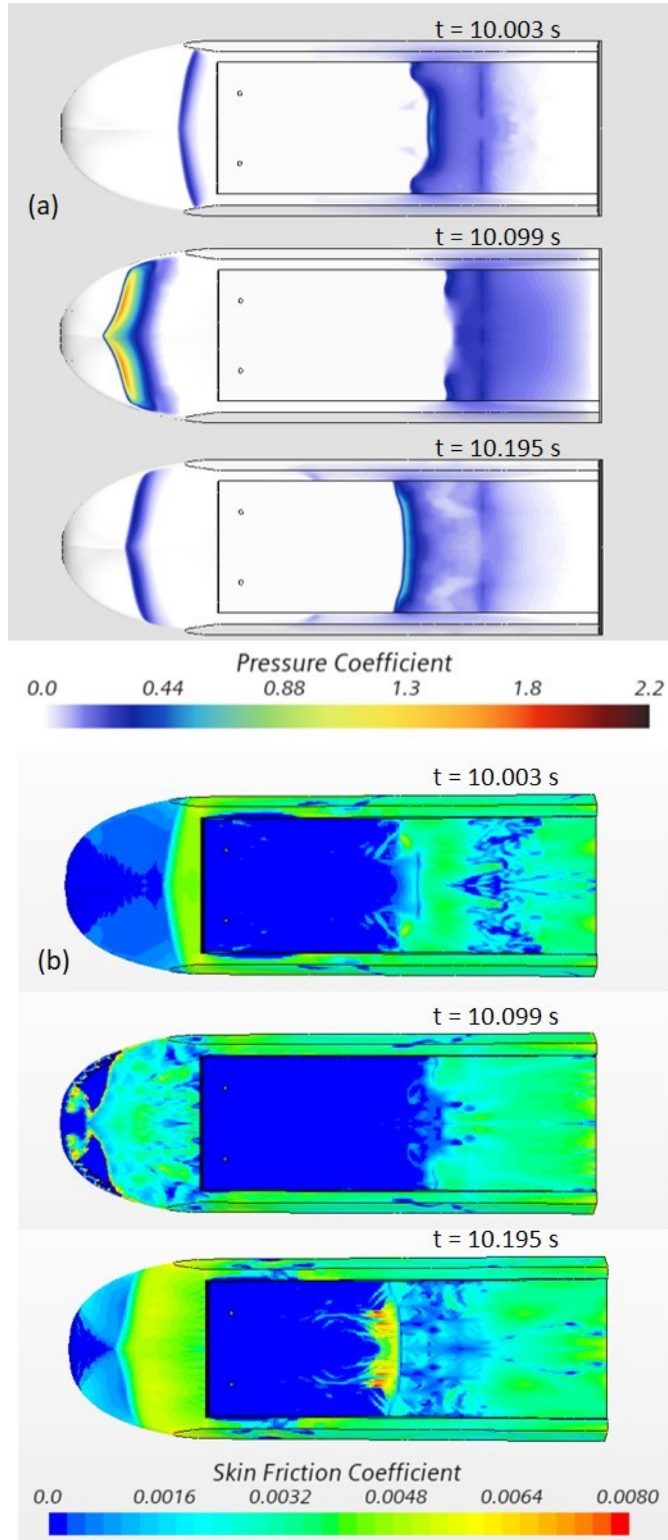

Fig. 10 Distributions of (a) pressure coefficient and (b) skin friction coefficient on the hull surface at three time instances in head waves with $\lambda = 1.09L$.

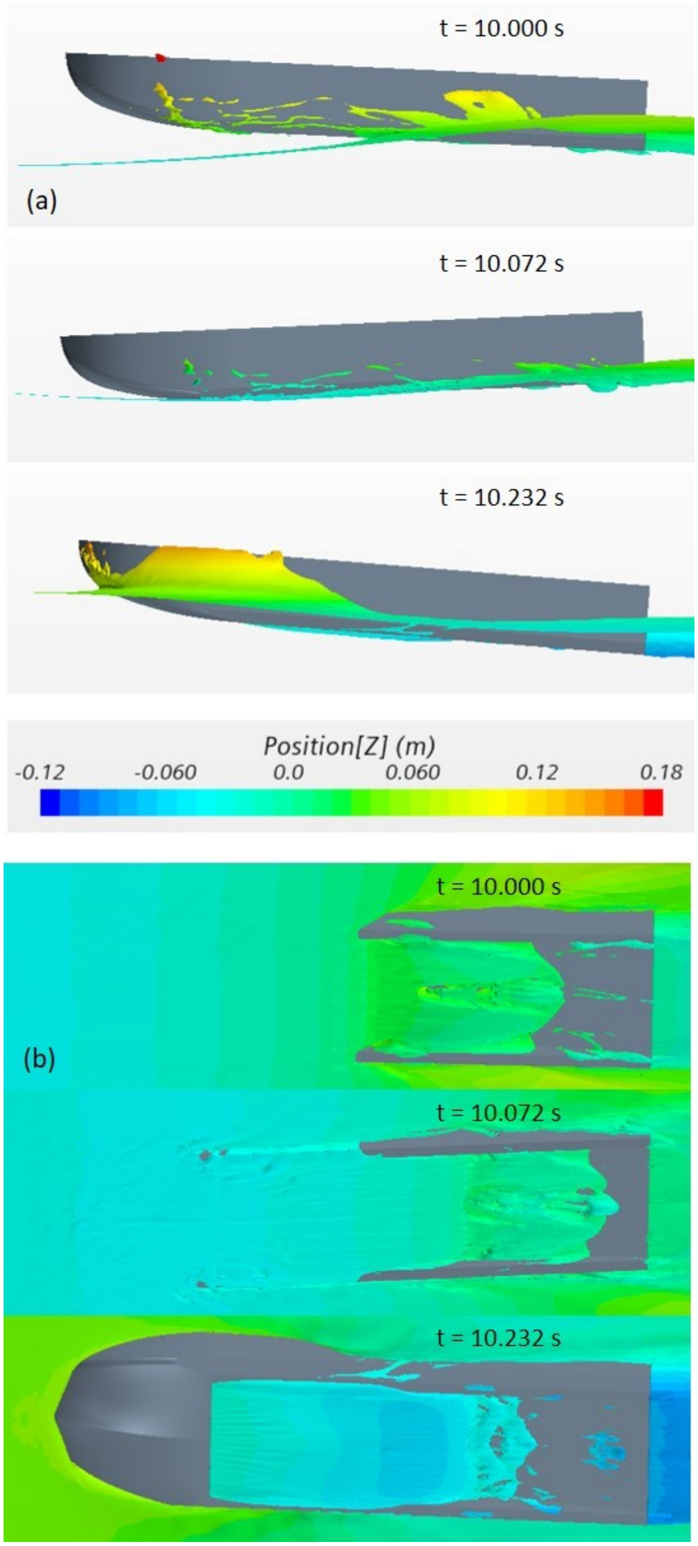

Fig. 11 Hull positions and wave surface elevations at three time instances in head waves with $\lambda = 2.18L$: (a) side view and (b) underwater view.

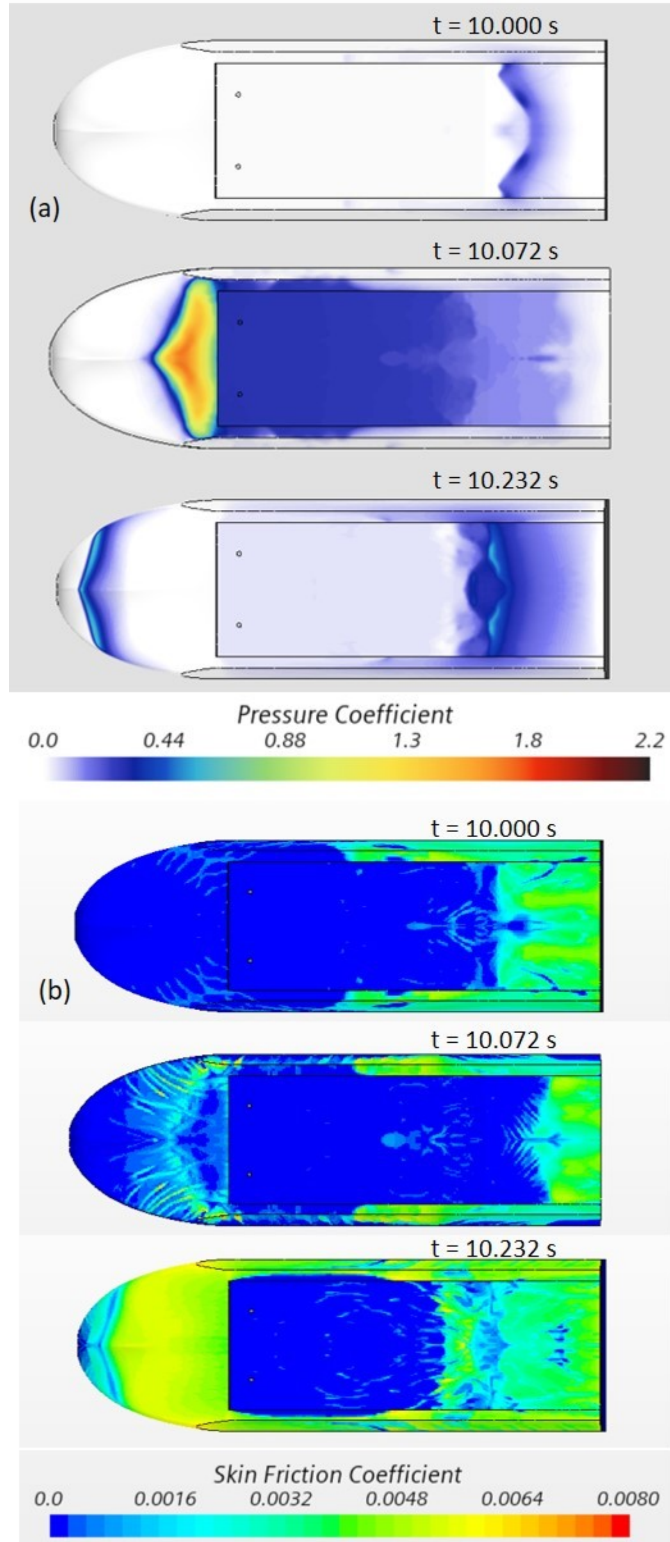

Fig. 12 Distributions of (a) pressure coefficient and (b) skin friction coefficient on the hull surface at three time instances in head waves with $\lambda = 2.18L$.

It is interesting to note that the average drag value in larger waves appears to be lower than in moderate waves (Table 3), although both values are substantially higher than in calm water. This artifact can be associated with higher averaged elevation and pitch of the hull in larger waves (Table 3). Nevertheless, bigger resistance in larger waves is expected to occur in practice due to surge motions, which are unaccounted here but inevitable in large waves. Also, significant reduction of propulsion efficiency will occur in such waves due to much larger oscillations of flow around propulsors and their closer proximity to the free water surface, so the overall propulsion power requirement will be significantly higher in larger waves.

The boat positions and distributions of flow variables in waves with $\lambda = 2.18L$ are shown in Figs. 11-12, which correspond to the time instances indicated by dashed lines in Fig. 8. In the first moment with large downward acceleration (approaching one g), more than half of the boat exits the wave crest (Fig. 11a). In the second time, the hull slams on water resulting in the upward (positive) peak acceleration exceeding two g's. As the boat moves through the next wave, it exhibits large pitch and spray at the bow.

The underwater images (Fig. 11b) demonstrate that a noticeable part of the bottom recess is exposed to the atmosphere in the initial time. As the boat slams on water, a thin air layer is trapped between the hull bow (and front parts of side skegs) and water at 10.072 s, whereas larger hull surface appears in the water in the third instant than in the case of smaller waves.

The pressure maps also indicate more dramatic changes in big waves (Fig. 12a). Only a small region in the hull aft has elevated pressure at 10 s. Significant pressure rise in the air cavity and on the wetted bow portion occurs at 10.072 s. In the third instant, deeper positioning of the hull with pressurized air-cavity and elevated pressure zones on the hull in the bow region and behind the cavity can be noticed in comparison with a similar phase in smaller waves (Fig. 10a). These observations suggest that the air cavity restores some of its lifting capabilities for at least a portion of a cycle in the case of larger waves. As shown in Fig. 12b, the friction patterns again correlate reasonably well with water surfaces (Fig. 11b) and show larger friction in the third instant.

Additional simulations in waves have been conducted for a solid hull with no bottom recess and no air supply but with otherwise the same geometry, loading and wave conditions. The RMS values for vertical accelerations and heave and pitch fluctuations are summarized in Table 4 for both solid and air-cavity hulls. The RMS values naturally increase in larger waves. The air-cavity hull experiences noticeably lower accelerations and heave motions, while its trim oscillation magnitudes are similar to those of the solid hull. These findings indicate that an air-filled bottom recess serves as an effective damper of vertical shocks, which is consistent with observations from previous drop experiments (Keehnel and Matveev 2014).

Table 4. RMS values of vertical accelerations and heave and pitch fluctuations of the air-cavity and solid hulls.

	Head waves, $\lambda = 1.09L$	Head waves, $\lambda = 2.18L$
Air-cavity hull		
a_{rms}	1.36 m/s^2	5.77 m/s^2
h'_{rms}	0.208 cm	2.47 cm
τ'_{rms}	0.600°	3.58°
Solid hull		
a_{rms}	3.03 m/s^2	7.49 m/s^2
h'_{rms}	0.431 cm	2.86 cm
τ'_{rms}	0.782°	3.10°

CONCLUSIONS

A computational study has been carried out for a wide-beam air-cavity hull in the semi-planing regime in the presence of regular head waves. In waves with a wavelength close to the hull length, about 24% increase of average drag was found, the boat vertical position and pitch decreased, and the air cavity lost its lifting capability, while still providing nearly friction-free zone on a portion of the hull bottom. In twice longer and higher waves, the hull exhibited 5-10 times larger oscillations in trim, pitch and vertical accelerations. High-frequency fluctuations in acceleration, which can be associated with air cavity oscillations, became more pronounced. As the boat average trim and heave increased, its average resistance became lower than in smaller waves, although ignored here surge motions and likely losses in propulsion efficiency are expected to result in much greater propulsive power required to maintain a semi-planing speed in larger waves. In comparison with a solid hull, the air-cavity boat exhibited substantially lower vertical accelerations and heave motions.

As for possible future research directions, one can investigate broader scope of operational conditions, include more degrees of freedom and propulsor models, and optimize hull geometry. Such studies will be computationally rather demanding if high fidelity in resolving air-ventilated flow features is needed. Experimental validation for both high-speed steady regimes and unsteady hull motions and air cavity dynamics is also highly desirable to provide confidence in the challenging for CFD simulations of air-cavity boats.

ACKNOWLEDGEMENTS

This material is based upon work supported by the National Science Foundation under Grant No. 1800135.

REFERENCES

Bertram, V. *Practical Ship Hydrodynamics*. Oxford: Butterworth-Heinemann, 2000.

Butuzov, A.A., Vasin, A.I., Drozdov, A.L., Ivanov, A.N., Kaluzhny, V.G., Matveev, I.I., and Ruzanov, V.E., “Full-Scale Trials of a Boat with an Air Cavity.”

Shipbuilding Problems, Series Ship Design, 28 (1981): 45-51.

Butuzov, A.A. “Spatial Linearized Problems on Flow around Ship with Artificial Cavitation.” *Shipbuilding Problems, Series Ship Design*, 8 (1988): 1-18.

Ceccio, S.L. “Friction Drag Reduction of External Flows with Bubble and Gas Injection.” *Annual Review of Fluid Mechanics*, 42 (2010): 183-203.

Collins, J.M., Whitworth, P.R., and Matveev, K.I., “Experimental Testing and Numerical Modeling of Small-Scale Boat with Drag-Reducing Air-Cavity System.” *Fluids Engineering Division Summer Conference*, ASME Virtual Conference, 2021. ASME paper FEDSM2021-62556.

Cucinotta, F., Guglielmino, E., Sfravara, F., and Strasser, C. “Numerical and Experimental Investigation of a Planing Air Cavity Ship and its Layer Evolution.” *Ocean Engineering,* 152 (2018): 130-144.

De Luca, F., Mancini, S., Miranda, S., and Pensa, C. “An Extended Verification and Validation Study of CFD Simulations for Planing Hulls.” *Journal of Ship Research*, 60:2 (2016): 101-118.

Faltinsen, O.M. *Hydrodynamics of High-Speed Marine Vehicles*. New York: Cambridge University Press, 2005.

Hao, W. “Numerical Study of the Effect of Ship attitude on the Perform of Ship with Air Injection in Bottom Cavity.” *Ocean Engineering*, 186 (2019): 106119.

Hirt, C.W., and Nichols, B.D. “Volume of Fluid (VOF) Methods for the Dynamics of Free Boundaries.” *Journal of Computational Physics*, 39:1 (1981): 201-225.

International Towing Tank Conference. *Uncertainty Analysis in CFD Verification and Validation Methodology and Procedures*. Publication 7.5-03-01-01, 2008.

Keehnel, D., and Matveev, K.I. “Drop Tests and Modeling of Water Entry of Air-Cavity Hull Sections,” *33rd International Conference on Ocean, Offshore and Arctic Engineering*, San Francisco, CA (2014). ASME paper no. OMAE2014-23060.

Latorre, R. “Ship Hull Drag Reduction Using Bottom Air Injection.” *Ocean Engineering*, 24 (1997): 161-175.

Lewison, G., and Maclean, W.M. “On the Cushioning of Water Impact by Entrapped Air.” *Journal of Ship Research*, 12:2 (1968): 116-130.

Matveev, K.I. “Modeling of Vertical Plane Motion of an Air Cavity Ship in Waves.” *5th International Conference on Fast Sea Transportation*, Seattle, USA (1999).

Matveev, K.I., and Dubrovsky, V.A., “Aerodynamic Characteristics of a Hybrid Trimaran Model.” *Ocean Engineering*, 34:3-4 (2007): 616-620.

Matveev, K.I. “Transom Effect on Properties of Air Cavity under Flat-Bottom Hull.” *Ships and Offshore Structures*, 7:2 (2012): 143-149.

Matveev, K.I., “Computational Modeling of Planing Hull Dynamics and Slamming in Head Waves.” *Fluids Engineering Division Summer Conference*, ASME Virtual Conference, 2021. ASME paper FEDSM2021-65548.

Matveev, K.I., and Collins, J.M. “Numerical Investigation of High-Reynolds-Number Air-Ventilated Water Flow under Solid Body with Surface Geometry Variations.” *Fluids*, (2021).

Mukha, T., and Bensow, R.E. “Flow Dynamics in the Closure Region of an Internal Ship Air Cavity.” *Ocean Engineering*, 216 (2020): 108192.

Pavlov, G.A., Yun, L., Bliault, A., and He, S.-L. *Air Lubricated and Air Cavity Ships: Development, Design and Application*. New York: Springer, 2020.

Rodi, W. “Experience with Two-Layer Models Combining the k-ε Model with a One-Equation Model near the Wall.” *29th Aerospace Sciences Meeting*, Reno, NV, USA, 1991. AIAA paper 91-0216.

Rotte, G., Kerkvliet, M., and van Terwisga, T. “Exploring the Limits of RANS-VoF Modeling for Air Cavity Flows.” *International Shipbuilding Progress*, 66 (2019): 273-293.

Yun, L., and Bliault, A. *Theory and Design of Air Cushion Craft*. Oxford: Elsevier, 2005.